

# Microstructure and Mechanical Properties of a Multiphase 17%Cr Stainless Steel

L.F. Noris<sup>a,b</sup>, S.S.M. Tavares<sup>a,b\*</sup> , A.R. Pimenta<sup>a,c</sup> , E.A. Ponzio<sup>d</sup>, J. M. Pardal<sup>a,b</sup>

<sup>a</sup>Universidade Federal Fluminense, Rua Passo da Pátria, 156, 24210-240, Niterói, RJ, Brasil.

<sup>b</sup>Universidade Federal Fluminense (UFF), Programa de Pós-Graduação em Engenharia Mecânica e Montagem Industrial, Escola de Engenharia, Rua Passo da Pátria, 156, 24210-240, Niterói, RJ, Brasil.

<sup>c</sup>Instituto Federal do Rio de Janeiro, Laboratório de Instrumentação e Simulação Computacional (LISCOMP), Campus Paracambi, Rua Sebastião Lacerda, 26600-000, Paracambi, RJ, Brasil.

<sup>d</sup>Universidade Federal Fluminense (UFF), Instituto de Química, Laboratório de Materiais (LaMUFF), Rua Outeiro de São João Batista, 24020-141, Niterói, RJ, Brasil.

Received: May 19, 2023; Revised: August 17, 2023; Accepted: October 02, 2023

The mechanical Properties of an experimental 17%Cr multiphase alloy were studied as function of heat treatment parameters. Containing majoritary ferrite and martensite, this type of steel is applied in tubullars and casings in the off shore oil and gas production, where high corrosion and mechanical resistance are required. Quenching and tempering heat treatments produced different combinations of ferrite, martensite, austenite and precipitates. The as quenched material has 35% of ferrite, martensite and 3.8% of retained austenite. The material quenched and tempered at 500°C has lower austenite (1.2%), and tempered martensite with Nb carbides. The tensile properties were excellent, but the low temperature (-46°C) impact toughness was very small. A high toughness was obtained in the material quenched and tempered at 650°C, with a microstructure of ferrite, tempered martensite and 7.2% of reversed austenite, but the mechanical resistance was under 621 Mpa (90ksi), which is considered too low for the application envisioned. The material tempered at 600°C showed an interesting combination of mechanical resistance and low temperature toughness. The flow stress curves of the material were modelled by Hollomon's equation and Voce's equation with correlation coefficients ( $R^2$ ) higher than 0.98.

**Keywords:** *mechanical properties, stainless steel, multiphase alloy, tempering.*

## 1. Introduction

The first supermartensitic stainless steels (SMSS's) were developed in the 1990's to obtain higher corrosion resistance, toughness, and weldability than conventional martensitic 12%Cr stainless steel. Considering the same 12%Cr base, the main compositional changes implemented were the drastic reduction of C content, and the Ni addition as  $\gamma$ -stabilizer<sup>1,2</sup>. Mo was introduced to increase the corrosion resistance, mainly localized corrosion resistance, and also to increase the mechanical resistance by retarding the softening due to tempering. Ti, V, or N microadditions are added to intensify secondary hardening and achieve yield classes 655 Mpa (95 ksi) and 758 MPa (110 ksi).

The primary use of supermartensitic stainless steels was as seamless tubes for off-shore oil and gas production, the so called oil country tubular goods (OCTG)<sup>2,3</sup>. For this application, a good combination of mechanical resistance, toughness, and corrosion resistance is necessary.

New alloys with higher Cr addition (14 to 17%) than SMSSs with 12-13%Cr are being developed and tested for OCTG application<sup>4,6</sup>. Other elements, such as V, W, and Cu, have been introduced in these new grades. The main objective of increasing Cr and adding Cu is to enhance the corrosion resistance of the alloy. However, the increase of ferritizing elements in the compositions introduces ferrite in the microstructure. Also, retained or reverse austenite

can be present, depending on the exact composition and the final heat treatment.

The corrosion resistance of an experimental 17%Cr alloy with ferrite, martensite, and austenite was investigated in previous works<sup>7-9</sup>. DL-EPR study showed that the degree of sensitization (DOS) is strongly influenced by the tempering parameters. Two peaks of DOS were detected at 550°C and 625°C, with an interesting healing process occurring in specimens tempered at 575°C and 600°C. Specimens tempered at 500°C or lower do not suffer sensitization in a 0.25 mol/L  $H_2SO_4$  + 0.01 mol/L KSCN solution<sup>7</sup>.

The pitting resistance was evaluated by polarization curves in 3.5%NaCl solution at 22°C. The pitting potential ( $E_{pit}$ ) was found to decrease slightly with the increase of tempering from 300°C to 650°C. The double tempering treatment provoked a further decrease in the  $E_{pit}$ . In all heat treatment conditions, the alloy suffered localized corrosion in the martensite due to its lower Cr and Mo contents<sup>8</sup>.

Up to now, there are few research papers reporting the properties of ferritic-martensitic stainless steels. The aim of this work was to study relationships between microstructure and mechanical properties of newly developed multiphase 17Cr steel for application in oil and gas production within high chloride media. It will be shown that the mechanical properties of the steel studied are strongly dependent on the final heat treatment, and much care must be taken to choose the correct treatment for the OCTG application.

\*e-mail: [ssmtavares@terra.com.br](mailto:ssmtavares@terra.com.br)

## 2. Experimental

The material studied in this work was from a seamless pipe, with the chemical composition shown in Table 1.

Specimens for tensile and impact Charpy tests were cut and roughly machined before heat treatments. Table 2 shows the heat treatments performed and the identification of specimens. After heat treatment, the specimens were machined to the final dimensions for tensile, hardness, and standard impact Charpy tests. Hardness and impact tests were performed in all conditions. Tensile tests were done in selected conditions, as indicated in Table 2.

Tensile and hardness tests were done at 22°C (± 1°C). The tensile specimen was machined to subsize dimensions (gauge length 16.0 mm and diameter 4.0 mm) of ASTM A370<sup>10</sup>. The tensile test was conducted with 0.5 mm/min velocity in an Instron 5582 with load cell 30 kN. Standard Charpy specimens (10x10x55 mm<sup>3</sup>) with V-notch were machined according to ASTM E-23<sup>11</sup>. Charpy impact tests were performed at 22°C and -46°C (± 1°C) in a Universal pendulum with 300 J of capacity. Vickers hardness was done with a load of 294.2 N (30 kgf). Eight hardness measurements were performed in each specimen, tensile tests were made in duplicate, and impact Charpy tests were made in triplicate.

For microstructural investigation in the light optical (LOM) and scanning electron microscopes (SEM), the specimens were prepared by grinding with emery paper, polishing with diamond paste, and etching with Vilella's reagent (95ml ethanol, 5ml HCl, and 1g picric acid). The ferrite volume fraction was measured by quantitative metallography in specimens observed by LOM, according to ASTM E562<sup>12</sup>. In addition, the microhardness was performed in ferrite and martensite phases individually. That test was performed in selected conditions, as indicated in Table 2, with a load of 0.490 N (50 gf).

The austenite phase may be present in quenched, and quenched and tempered conditions, but the quantification of this phase by microscopy is not precise. The method chosen to determine the austenite volume fractions (AVF) was based on the magnetization saturation ( $m_s$ ) of a Vibrating Sample Magnetometer (VSM).

Small disc specimens with 3.5 mm diameter and 0.5 mm thickness were machined and cut. The magnetizations curves were obtained at room temperature in the VSM, with a maximum applied field (H) of 1.5 T. The  $m_s$  was determined by the extrapolation of the magnetization versus the 1/H curve to 1/H → 0. The austenite volume fraction (AVF) was determined by Equation 1:

$$AVF = 1 - \frac{m_s}{m_{s(i)}} \quad (1)$$

Where  $m_s$  is the magnetization saturation of the specimen analyzed, and  $m_{s(i)}$  is the intrinsic saturation magnetization of martensite/ferrite. As a simplification of the method, it was considered that these two magnetic phases (ferrite and martensite) have the same  $m_{s(i)}$ , which corresponds to the  $m_s$  of a specimen without any detectable austenite. This specimen was produced by quenching from 1000°C to -196°C. Three magnetic measurements per specimen were performed.

## 3. Results and Discussion

Figure 1 shows the behavior of impact toughness measured at room temperature (RT) (22°C) and -46°C.

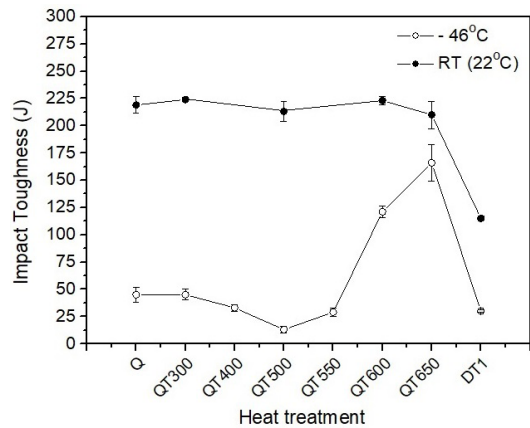


Figure 1. Impact tests results at RT and -46°C.

Table 1. Chemical composition of the steel studied [wt. %].

C	Cr	Mo	Ni	Si	Mn	Cu	W	Nb	P	S	N
0.027	16.58	2.38	3.42	0.223	0.318	0.941	1.89	0.100	0.023	0.003	0.025

Table 2. Heat treatments and mechanical tests performed (H = hardness, I = Impact Charpy, T = tensile, M = microhardness).

Identification	Heat treatment description	Tests
Q	Quenched (soaking at 1000°C/1h, water cooling)	H, I, T, M
QT300	Quenched and tempered at 300°C	H, I
QT400	Quenched and tempered at 400°C	H, I
QT500	Quenched and tempered at 500°C	H, I, T, M
QT550	Quenched and tempered at 550°C	H, I
QT600	Quenched and tempered at 600°C	H, I, T
QT650	Quenched and tempered at 650°C	H, I, T, M
DT	Quenched & double tempered (670°C/2h+620°C/2h)	H, I

In general, all specimens present very high toughness at RT, but a considerable decrease is observed in the specimen double tempered (DT). The toughness at RT can be compared to values measured by Wen<sup>13</sup> in an AISI 403 stainless steel with a dual phase ferritic-martensitic microstructure, and the values obtained in this work are much superior due to the lower carbon content, 0.028% against 0.1%, and the Ni addition to the SMSS. In tests performed at -46°C, the results were considerably lower, mainly in the specimen QT-500.

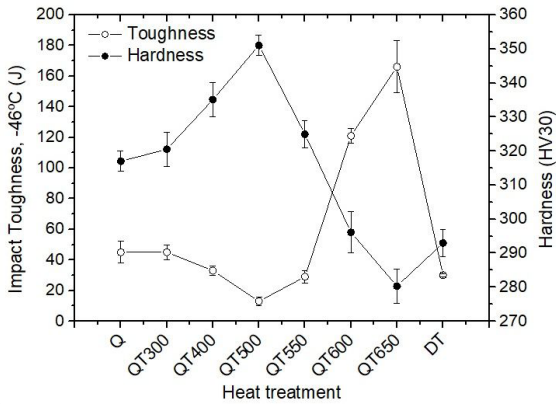


**Figure 2.** Toughness at -46°C and hardness as a function of heat treatment.

However, an interesting increase of toughness is observed with the increase of tempering temperature above 550°C, reaching a peak at 650°C. The double tempered steel was very low, confirming the trend observed in the tests at RT. In Figure 2, the hardness and the impact toughness at -46°C data were put in the same graph. The material has an increase of hardness in specimens tempered between 300 and 550°C, which is characteristic of secondary hardening. The peak of hardness and minimum toughness at -46°C were coincident and occurred in the specimen tempered at 500°C (QT-500). Figures 3a-c show the fracture surfaces of specimens Q, QT500, and DT tested at -46°C, and it is possible to see quasi-cleavage features in all. In contrast, specimen QT650 showed dimples and ductile behavior (Figure 3d). Similar results were observed in a Ti-alloyed SMSS, which presented temper embrittlement in the 400-600°C range<sup>14,15</sup>.

Microstructures of specimens Q, QT-500, and QT-650 observed in the LOM are shown in Figures 4a, 4b, 5a, 5b, and 6a, 6b, respectively. The as quenched material (Q) has an apparent biphasic structure with  $\delta$ -ferrite volume fraction equal to  $0.35 \pm 0.02$ , as measured by quantitative metallography using 10 images with the same magnification of Figure 4a. The amount of  $\delta$ -ferrite didn't vary significantly with the tempering temperature. Besides  $\delta$ -ferrite and martensite, the steel also contains austenite within the martensite islands, which could not be distinguished or quantified by microscopy (LOM and SEM). The austenite volume fractions (AVF) determined by the magnetic method are depicted in Figure 7.

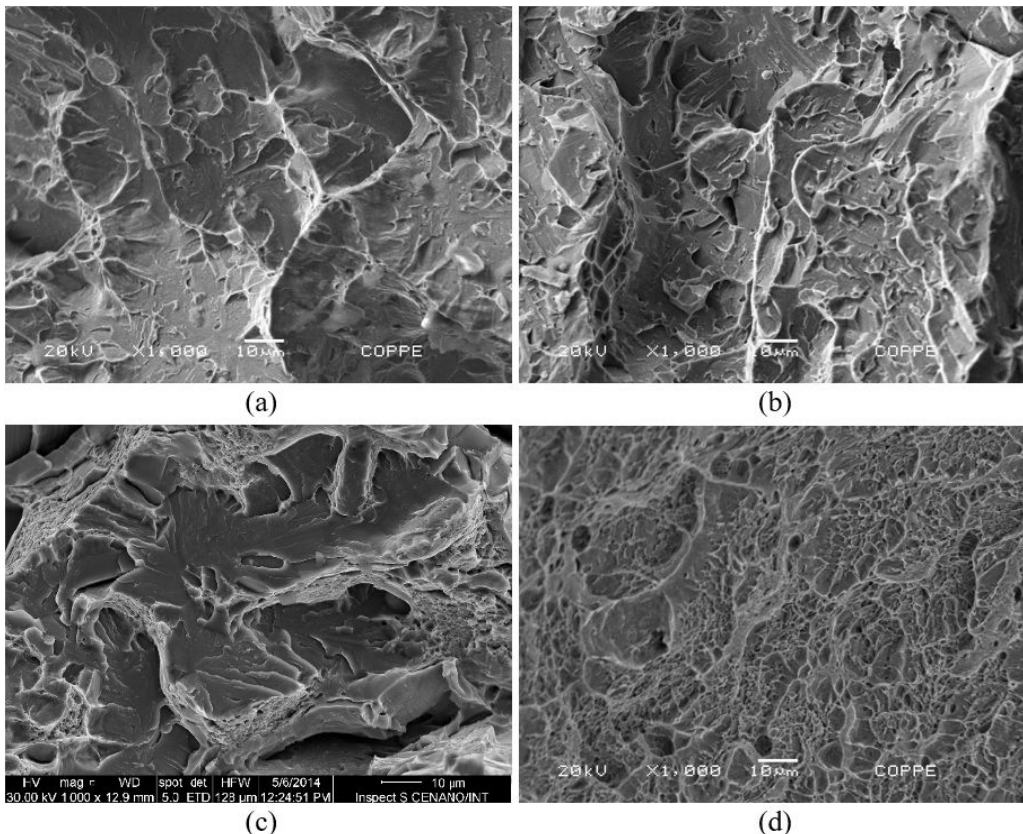


**Figure 3.** Fractography of impact Charpy specimens tested at -46°C: (a) Q; (b) QT500; (c) DT; (d) QT650.

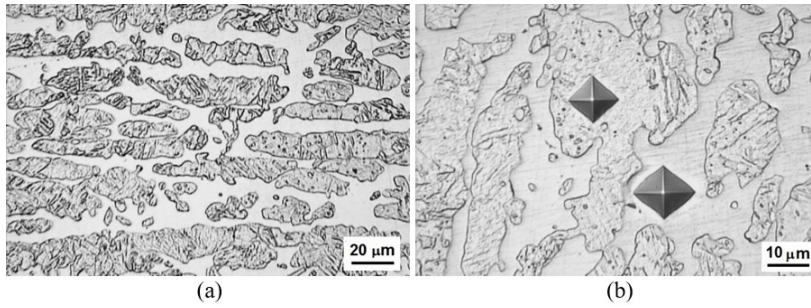


**Figure 4.** Microstructure of specimen Q observed in the LOM: (a) general view; (b) image with microhardness identifications.

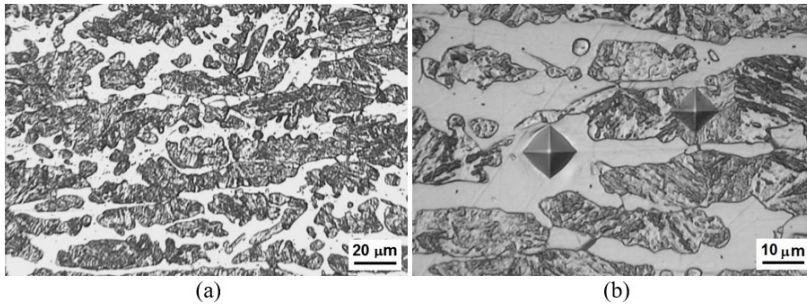


**Figure 5.** Microstructure of specimen QT500 observed in the LOM: (a) general view; (b) image with microhardness identifications.

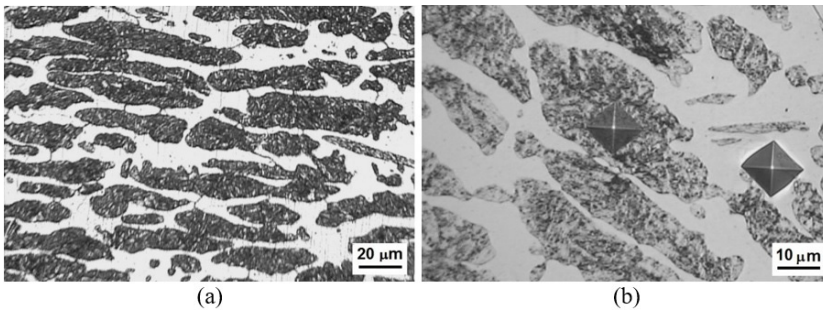


**Figure 6.** Microstructure of specimen QT650 observed in the LOM: (a) general view; (b) image with microhardness identifications.

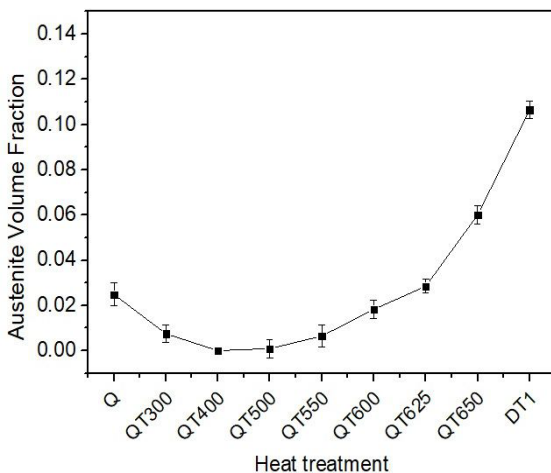


**Figure 7.** AVF as a function of the heat treatment.

The as quenched specimen has 3.8% of retained austenite, which is converted in fresh martensite during the tempering at 300°C. Ni, Mn, and other elements decrease the  $A_1$  temperature, and the tempering carried out above  $A_1$  causes the reversion of martensite to austenite during the tempering. As a consequence, the austenite content increases with the tempering temperature above 400°C, due to the formation of reverse austenite. In single tempering treatments the reverse austenite reaches 7.4% in specimen QT-650. The double tempering treatment causes a further increase of austenite to 13.6%, indicating a behavior very similar to supermartensitic stainless steels 12-13%Cr<sup>14,15</sup>.

Microhardness measurements of ferrite and martensite islands of specimens Q, QT-500 and QT-650 were measured as shown in Figures 4b, 5b, and 6b. Figure 8 shows that the secondary hardening in the tempering treatment between 400 and 550°C (see Figure 2), with peak at 500°C, is also observed in the microhardness results.

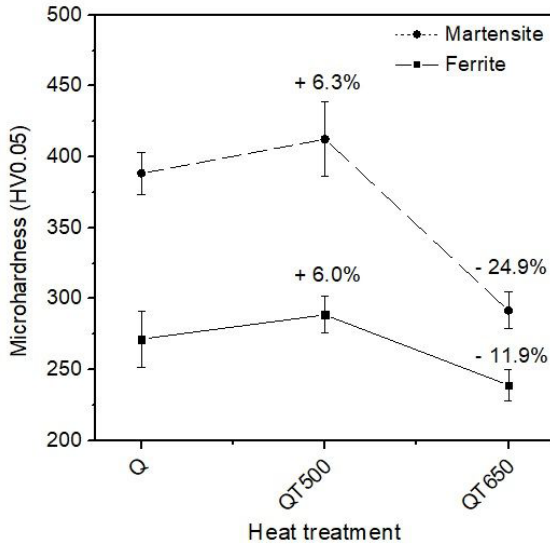


Figure 8. Microhardness as a function of the heat treatment.

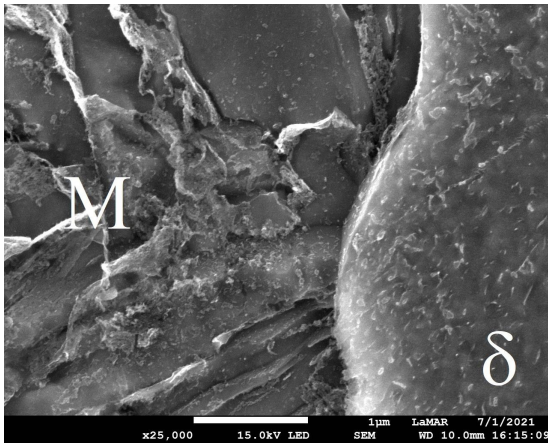


Figure 9. SEM image of specimen QT-500.

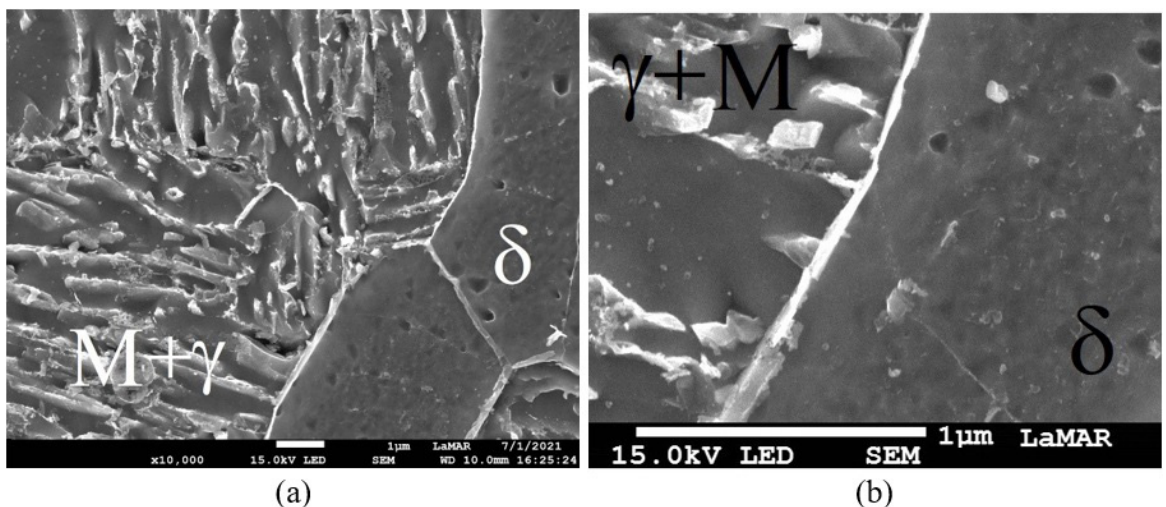


Figure 10. Microstructures of specimen QT-650: (a) general view; (b) details of precipitates in ferrite ( $\delta$ ) and in tempered martensite ( $\gamma+M$ ).

Not only the martensite phase is hardened by precipitation reactions in the tempering at 500°C, but also the ferrite phase. Figures 9 shows in detail the microstructure of specimen QT-500, where fine precipitates are observed in the ferrite and martensite islands. The austenite content is very small (1.2%). The chemical composition of fine precipitates could not be analyzed by EDS (energy dispersive spectroscopy). The steel studied contains Nb and W micro-additions to form carbides and carbonitrides. In a previous work of our group, X-ray diffraction analysis was carried out in precipitates extracted by electrolytic dissolution of the matrix of specimens tempered at 500°C (QT-500) and 650°C (QT-650)<sup>9</sup>. NbC and Nb(C,N) reflections were observed in the specimen QT-500, and Cr carbides and NbC/Nb(C,N) were detected in QT-650. Figures 10a and 10b shows the precipitates in specimen QT-650. The intragranular precipitates in QT-650 are coarser than in QT-500, and the intergranular precipitates are likely the Cr carbides detected in XRD analysis. These features contribute to the higher toughness and lower hardness of specimen QT-650 compared to QT-500. It is also possible that the austenite phase, representing 7.4% of the microstructure of QT-650, has a positive effect on the impact toughness. The very low toughness of QT-500 denotes a kind of temper embrittlement which may be related to the fine precipitates that increase the hardness.

The lower toughness observed in specimen DT may be attributed to the precipitation of intermetallics. Garcia et al.<sup>6</sup> produced a specimen with 6% chi phase ( $\chi$ ), 7% of austenite ( $\gamma$ ), 33% of ferrite ( $\delta$ ), and 66% of martensite (M) by heat treating a 14%Cr-3%Mo steel at 670°C for 18h. Jeon et al.<sup>16</sup> concluded that the W addition slightly increases chi phase formation for duplex stainless steel. Similar behavior may be occurring in a SMSS studied in this work. SEM analysis of specimen DT is shown in Figure 11. It can be observed bright particles in the ferrite and in the tempered martensite. Also, intergranular precipitation is observed. These precipitates could not be analyzed by EDS due to the small size.

Apparently, the toughness of specimen DT is lowered by the intergranular precipitates. These precipitates have harmful effects and must be avoided. The intergranular precipitation, probably of Cr carbides, does not embrittle the steel, since they were also present in the very tough QT-650. Corroborating this finding, the fracture surface of specimen DT shows predominantly quasi-cleavage facets, microvoids and tearing (Figure 3c), without intergranular cracks. It is also worth mentioning that the high austenite content (13.6%) does not counterbalance the embrittlement effect of precipitates in specimen DT.

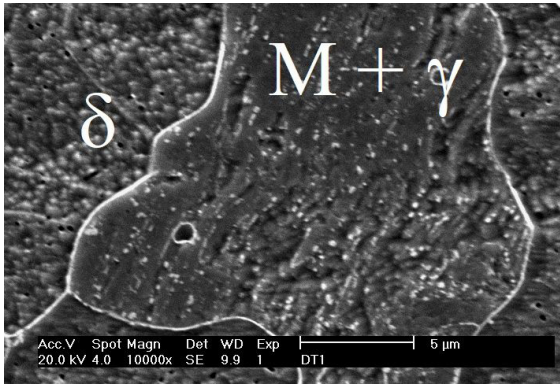


Figure 11. Microstructure of specimen DT showing bright intergranular and intragranular precipitates.

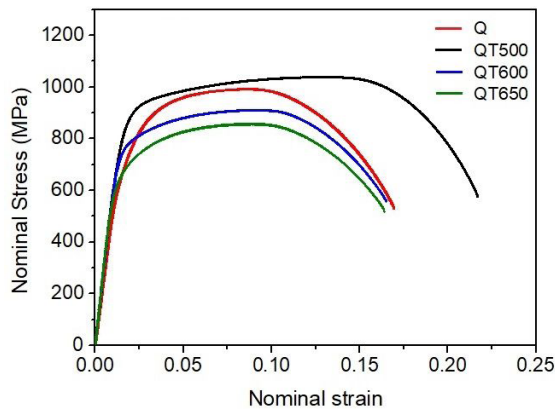


Figure 12. Engineering curves of specimens Q, QT-500, QT-600, and QT-650.

After microstructural analysis and toughness and hardness results, four conditions were selected for tensile tests, Q, QT-500, QT-600, and QT-650. Figure 12 compares the tensile curves, and Table 3 shows the tensile properties obtained. Hardness results were also included. The highest yield strength obtained was 801 MPa in the specimen QT-500. Only in this heat treatment condition, the material achieved the properties of class 758 MPa (110 ksi) of yield stress. Surprisingly, the elongation was higher in this condition, and, as a consequence, the area of the  $\sigma\epsilon$  curve was also superior to the others. However, the toughness at  $-46^{\circ}\text{C}$  was minimum (13J) in specimen QT-500, denoting a temper embrittlement only detected at low temperature impact tests. The material will probably not be selected for such low temperatures. For use in the ambient temperature or higher, the toughness is high, as shown in Figure 1. On the other hand, the resistance to hydrogen embrittlement at this condition may be lower than in the other tempering conditions<sup>9</sup>.

Condition QT-650 gives the higher toughness at  $-46^{\circ}\text{C}$ , but the yield strength is too low ( $< 621$  MPa, 90Ksi). The tempering condition of specimen QT-600 may be an optimum choice between QT-500 and QT-650 since the toughness at  $-46^{\circ}\text{C}$  is high (125J) and the yield strength is compatible to class 655 MPa (95 ksi). The lower hardness of QT-600 also indicates a better resistance to sulfide stress corrosion than QT-500<sup>17</sup>, but this was not tested till now.

The true stress *versus* true strain curves were modeled by constitutive equations of Hollomon (2)<sup>18</sup>, Ludwik (3)<sup>19</sup>, and Voce (4)<sup>20</sup>:

$$\sigma = K_H \cdot \epsilon^{n_H} \quad (2)$$

$$\sigma = \sigma_o + K_L \cdot \epsilon^{n_L} \quad (3)$$

$$\sigma = \sigma_o + a \cdot \epsilon + b(1 - \exp(-c \cdot \epsilon)) \quad (4)$$

where  $K_H$ ,  $K_L$ ,  $n_H$ , and  $n_L$  are independent parameters in Equations 2 and 3, and  $a$ ,  $b$ , and  $c$  are independent parameters in Equation 4. Also, Equations 3 and 4  $\sigma_o$  is the proportional limit, or the exact point separating elastic and plastic regimes.

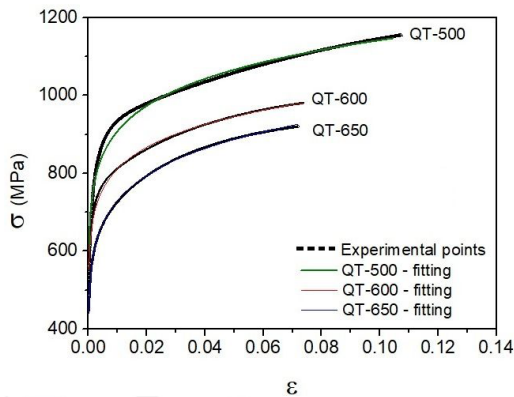
Table 4 shows the results of modeling with Equations 2, 3 and 4. The goodness of the fitting may be measured by the correlation coefficient  $R^2$ . Despite its simplicity, Hollomon's equation gave excellent results for the 17%Cr studied, better than Ludwik's equation in all conditions and better than Voce's equation in conditions QT-600 and QT-650. Figure 13 shows the flow curves of QT-500, QT-600, and QT-650 adjusted with Hollomon's equation.

Table 3. Tensile Properties and hardness of Q, QT-500, QT-600, and QT-650.

Specimen	$\sigma_{YS}$ , MPa (ksi)	$\sigma_{UTS}$ , MPa (ksi)	Elongation	Area $\sigma\epsilon$ , MPa	Hardness HV10
Q	637 (91)	993 (141)	0.1590	142	317 $\pm$ 3
QT-500	801 (115)	1037 (148)	0.2075	200	351 $\pm$ 2
QT-600	721 (103)	911 (130)	0.1568	132	296 $\pm$ 5
QT-650	616 (88)	856 (123)	0.1556	122	280 $\pm$ 4

**Table 4.** Parameters of Hollomon, Ludwik, and Voce's equations for Q, QT-500, QT-600, and QT-650.  $K_H$ ,  $K_L$ ,  $\sigma_o$ , a, and b are given in MPa.

Sample	Hollomon (Equation 2)			Ludwik (Equation 3)				Voce (Equation 4)				
	$K_H$	$n_H$	$R^2$	$\sigma_o$	$K_L$	$n_L$	$R^2$	$\sigma_o$	a	b	c	$R^2$
Q	1585	0.139	0.987	503	1501	0.335	0.953	503	2652	401	171	0.997
QT500	1435	0.099	0.987	560	1034	0.242	0.960	560	2188	379	381	0.995
QT600	1256	0.095	0.998	521	946	0.266	0.974	521	2700	283	497	0.987
QT650	1269	0.112	0.999	446	1105	0.305	0.982	446	2860	292	284	0.983

**Figure 13.** True stress x true strain curves with Hollomon's fittings.

#### 4. Conclusions

The relations between microstructural and mechanical properties of a 17%Cr multiphase stainless steel submitted to different heat treatments were investigated. The main conclusions are:

- The as quenched material (Q) contains approximately 35.0% ferrite, 61.2% of martensite, and 3.8% of retained austenite. Since the austenite phase is inside the martensite phase, and could not be identified by LOM or conventional SEM, its quantification was assessed by magnetic measurements.
- The ferrite content did not change significantly with the tempering treatments. The material quenched and tempered at 500°C (QT-500) has ferrite, tempered martensite, and traces of austenite (1.2%). Fine precipitates, probably Nb(C,N), were observed in the ferrite and austenite. At this condition, the hardness and mechanical resistance were maximum, achieving the class 758 MPa (110ksi) of yield strength. However, the material presented a brittle behavior in the impact test at -46°C.
- Specimen quenched and tempered at 650°C (QT-650) has a microstructure of ferrite, tempered martensite, and 7.4% of reversed austenite. Nb(C,N) and Cr carbides are also present. At this heat treatment condition, the material showed high toughness at -46°C, but the lowest yield strength (616 MPa, 88 ksi).
- Specimen quenched and tempered at 600 °C (QT-600) has mechanical properties intermediary between QT-500 and QT-650, and can be a good option to obtain a material with yield class 655 MPa (95 ksi), and high impact toughness.

- Double tempering treatment results in low toughness due to and intragranular precipitation and, for this reason, must be avoided.
- True stress *versus* true strain curves of specimens QT-500, QT-600, and QT-650 were modeled by Hollomon's, Ludwik's, and Voce's equations. The Hollomon model, despite its simplicity, presented excellent results, as measured by correlation coefficients  $R^2$ .

#### 5. Acknowledgments

Authors acknowledge Brazilian research agencies CNPq (308244/2022-2) and FAPERJ (E-26/200.423/2023, E-26/200.122/2023, and E26/211.412/2021) for financial support.

#### 6. References

1. Olden V, Thaulow C, Johnsen R. Modelling of hydrogen diffusion and hydrogen induced cracking in supermartensitic and duplex stainless steels. *Mater Des.* 2008;29(10):1934-48. <http://dx.doi.org/10.1016/j.matdes.2008.04.026>.
2. Barbosa C, Abud I. Recent developments on martensitic stainless steels for oil and gas production. *Recent Pat Corros Sci.* 2013;3(1):27-38. <http://dx.doi.org/10.2174/22106839112029990004>.
3. Davis JR. *ASM speciality handbook: stainless steels.* Ohio: ASM International; 1994.
4. Kimura M, Tamari T, Yamazaki Y, Sakata K, Mochizuki R, Sato H. Development of new 15Cr stainless steel OCTG with superior corrosion resistance. In: *SPE Applied Technology Workshop on High Pressure/High Temperature Sour Well Design; 2005; The Woodlands, Texas. Proceedings.* Texas: Society of Petroleum Engineers; 2005.
5. Kimura M, Tamari T, Ken S. High Cr stainless steel OCTG with high strength and superior corrosion resistance. *JFE Tech Rep.* 2006;3:7.
6. Garcia DCS, Carvalho RN, Lins VFC, Rezende DM, Santos DS. Influence of microstructure in the hydrogen permeation in martensitic-ferritic stainless steel. *Int J Hydrogen Energy.* 2015;40(47):17102-9. <http://dx.doi.org/10.1016/j.ijhydene.2015.06.102>.
7. Tavares SSM, Sampaio MTG, Peres G, Almeida BB, Ponzio EA. DL-EPR and AFM study of sensitization of a 17%Cr multiphase stainless steel. *Materials and Corrosion.* 2022;73(6):866-75. <http://dx.doi.org/10.1002/maco.202112814>.
8. Pardal JM, Da Silva MR, Bastos IN, Macêdo MCS, Tavares SSM. Influence of tempering treatment on microstructure and pitting corrosion resistance of a new super ferritic-martensitic-austenitic stainless steels with 17%Cr. *Corros Eng Sci Technol.* 2016;51(5):337-41. <http://dx.doi.org/10.1080/1478422X.2015.1110418>.

9. Tavares SSM, Bastos IN, Pardal JM, Montenegro TR, Silva MR. Slow strain rate tensile test results of new multiphase 17%Cr stainless steel under hydrogen cathodic charging. *Int J Hydrogen Energy*. 2015;40:16992. <http://dx.doi.org/10.1016/j.ijhydene.2015.05.148>.
10. ASTM: American Society for Testing and Materials. ASTM A370: standard test methods and definitions for mechanical testing of steel products. West Conshohocken: ASTM International; 2022. <http://dx.doi.org/10.1520/A0370-21>.
11. ASTM: American Society for Testing and Materials. ASTM E23: standard test methods for notched bar impact testing of metallic materials. West Conshohocken: ASTM International; 2018. <http://dx.doi.org/10.1520/E0023-18>.
12. ASTM: American Society for Testing and Materials. ASTM E562: standard test method for determining volume fraction by systematic manual point count. West Conshohocken: ASTM International; 2020.
13. Wen DC. Improvement of slurry erosion resistance of martensite/ferrite duplex stainless steel by hot rolling. *Met Mater Int*. 2010;16(1):13-9. <http://dx.doi.org/10.1007/s12540-010-0013-z>.
14. Silva GF, Tavares SSM, Pardal JM, Silva MR, Abreu HFG. Influence of heat treatments on toughness and sensitization of a Ti-alloyed supermartensitic stainless steel. *J Mater Sci*. 2011;46(24):7737-44. <http://dx.doi.org/10.1007/s10853-011-5753-8>.
15. Tavares SSM, Pardal JM, Souza GC, Oliveira CAS, Abreu HFG. Influence of tempering on microstructure and mechanical properties of Ti alloyed 13%Cr supermartensitic stainless steel. *Mater Sci Technol*. 2014;30(12):1470-6. <http://dx.doi.org/10.1179/1743284713Y.0000000448>.
16. Jeon S, Kim S, Lee I, Kim J, Kim K, Park Y. Effects of W substitution on the precipitation of secondary phases and the associated pitting corrosion in hyper duplex stainless steels. *J Alloys Compd*. 2012;544:166-72. <http://dx.doi.org/10.1016/j.jallcom.2012.07.129>.
17. NACE: National Association of Corrosion Engineers. NACE ISO 15156-3: petroleum and natural gas industries - materials for use in H<sub>2</sub>S-containing environments in oil and gas production. Part 3: cracking-resistant CRAs (corrosion-resistant alloys) and other alloys. Geneva: NACE International; 2015.
18. Hollomon JH. Tensile deformation. *Trans AIME*. 1945;162:268.
19. Ludwik P. *Element der Technologischen Mechanik*. Berlin: Springer; 1909.
20. Voce E. The relationship between stress and strain for homogeneous deformation. *J Inst Met*. 1948;74:537.